SEARCH PROCEEDINGS

Search

Advanced Search

BROWSE PROCEEDINGS
- Proceedings
  - By Year
  - By Symposium
  - By Volume No.
  - By Volume Title
  - By Technology

BROWSE JOURNALS
- Journals
  - Optical Engineering
  - J. Electronic Imaging
  - J. Biomedical Optics
  - J. Micro/ Nanolithography, MEMS, and MOEMS
  - J. Applied Remote Sensing
  - J. Nanophotonics
  - SPIE Letters Virtual Journal

SUBSCRIPTIONS & PRICING
- Institutions & Corporations
- Personal subscriptions

GENERAL INFORMATION
- About the Digital Library
- Terms of Use
- SPIE Home

Proc. SPIE / Volume 7261 / Cardiac

PREV NEXT

Model-driven physiological assessment of the mitral valve from 4D TEE

Proc. SPIE, Vol. 7261, 72610R (2009); DOI:10.1117/12.812096

Online Publication Date: 13 March 2009

Conference Date: Sunday 8 February 2009
Conference Location: Lake Buena Vista, FL, USA
Conference Title: Medical Imaging 2009: Visualization, Image-Guided Procedures, and Modeling
Conference Chairs: Michael I. Miga, Kenneth H. Wong

ABSTRACT | REFERENCES (12)

Ingmar Voigt
Siemens Corporate Technology (Germany) and Friedrick-Alexander-Univ. (Germany)

Razvan Ioan Ionasec
Siemens Corporate Research (USA) and Technical Univ. Munich (Germany)

Bogdan Georgescu
Siemens Corporate Research (USA)

Helene Houle
Siemens Medical Solutions (USA)

Disorders of the mitral valve are second most frequent, cumulating 14 percent of total number of deaths caused by Valvular Heart Disease each year in the United States and require elaborate clinical management. Visual and quantitative evaluation of the valve is an important step in the clinical workflow according to experts as knowledge about mitral morphology and dynamics is crucial for interventional planning. Traditionally this involves examination and metric analysis of 2D images comprising potential errors being intrinsic to the method. Recent commercial solutions are limited to specific anatomic components, pathologies and a single phase of cardiac 4D acquisitions only. This paper introduces a novel approach for morphological and functional quantification of the mitral valve based on a 4D model estimated from ultrasound data. A physiological model of the mitral valve, covering the complete anatomy and eventual shape variations, is generated utilizing parametric spline surfaces constrained by topological and geometrical prior knowledge. The 4D model's parameters are estimated for each patient using the latest discriminative learning and incremental searching techniques. Precise evaluation of the anatomy using model-based dynamic measurements and advanced visualization are enabled through the proposed approach in a reliable, repeatable and reproducible manner. The efficiency and accuracy of the method is demonstrated through experiments and an initial validation based on clinical research results. To the best of our knowledge this is the first time such a patient specific 4D mitral valve model is proposed, covering all of the relevant anatomies and enabling to model the common pathologies at once.

DOI Link: http://dx.doi.org/10.1117/12.812096

PROCEEDINGS DATA

ISSN:

0277-786X (print)

Publisher:

SPIE

crossref Member

Model-driven physiological assessment of the mitral valve from 4D TEE

Ingmar Voigt[a,e], Razvan Ioan Ionasec[b,c], Bogdan Georgescu[b], Helene Houle[d], Martin Huber[a] , Joachim Hornegger[e] and Dorin Comaniciu[b]

[a] Siemens Corporate Technology, Software & Engineering SCR 2, Erlangen, Germany
[b] Integrated Data Systems, Siemens Corporate Research, Princeton, NJ, USA
[c] Computer Aided Medical Procedures, Technical University Munich, Germany
[d] Siemens Medical Solutions, Innovations Ultrasound, Mountain View, CA, USA
[e] Chair of Pattern Recognition, Friedrich-Alexander-University, Erlangen, Germany

ABSTRACT

Disorders of the mitral valve are second most frequent, cumulating 14 percent of total number of deaths caused by Valvular Heart Disease each year in the United States and require elaborate clinical management. Visual and quantitative evaluation of the valve is an important step in the clinical workflow according to experts as knowledge about mitral morphology and dynamics is crucial for interventional planning.[1,2] Traditionally this involves examination and metric analysis of 2D images comprising potential errors being intrinsic to the method. Recent commercial solutions are limited to specific anatomic components, pathologies and a single phase of cardiac 4D acquisitions only. This paper introduces a novel approach for morphological and functional quantification of the mitral valve based on a 4D model estimated from ultrasound data. A physiological model of the mitral valve, covering the complete anatomy and eventual shape variations, is generated utilizing parametric spline surfaces constrained by topological and geometrical prior knowledge. The 4D model's parameters are estimated for each patient using the latest discriminative learning and incremental searching techniques. Precise evaluation of the anatomy using model-based dynamic measurements and advanced visualization are enabled through the proposed approach in a reliable, repeatable and reproducible manner.[3] The efficiency and accuracy of the method is demonstrated through experiments and an initial validation based on clinical research results. To the best of our knowledge this is the first time such a patient specific 4D mitral valve model is proposed, covering all of the relevant anatomies and enabling to model the common pathologies at once.

Keywords: physiological valve modeling, model based quantitative & visual assessment, discriminative learning

1. INTRODUCTION

Mitral valve disease represents the second most common valvular disease in developed countries.[4] Minimally invasive mitral valve repair procedures are mostly under development or in trial yielding the need for precise knowledge and reliable display of the four-dimensional valve characteristics. Computed tomography and 4D ultrasound are modalities well suited for non-invasive imaging of the heart enabling dynamic four-dimensional evaluation of cardiac structures throughout the cardiac cycle. Still those data sets still have to be viewed as 2D images used to perform measurements, which is an elaborate procedure and potentially error prone considering the fact that for example the mitral valve's annulus or the mitral valvular orifice is a non-planar curve. A four dimensional model derived from ultrasound data sets offers the unique possibility to non-invasively visualize and quantify the dynamics of the mitral annulus and leaflets in functional and diseased valves. Existent valve models presented in the literature[5–7] are used for hemodynamic studies or analysis of prostheses. Although some of them are generated from volumetric data, these models are generic and obviously not applicable for the evaluation of individual patients. Further related academic work and commercial solutions[8–12] focus mainly on certain aspects, such as isolated parts of the anatomy, certain pathologies and related measurements, but do not provide such four-dimensional model, covering the full mitral valve anatomy, with precisely discriminated components and their dynamics, and all pathologies at once.

Further author information: Ingmar Voigt: E-mail: ingmar.voigt.ext@siemens.com

In this paper we introduce a new modeling framework for the mitral valve from 4D cardiac ultrasound data. A dynamic model of the valve is constructed from anatomic structures together with physiology driven geometrical and topological constraints. The patient specific parameters of the model are estimated from ultrasound data by combining learning-based technologies into a multi-stage, coarse-to-fine parameter estimation algorithm. The estimated model enables for the first time precise morphological and functional quantification as well as enhanced visualization of the mitral valve. Extensive experiments on 30 patients with various valvular disorders demonstrate the accuracy and speed of the proposed model estimation algorithm. Initial clinical validation on various functional and pathological valves shows a strong correlation among a proposed set of model-based measurements, manually performed measurements and previously reported mitral valve dimensions.

2. MITRAL VALVE MODELING

We propose a physiology driven parametric 4D model capable to express a large spectrum of morphological and pathological variations of the mitral valve. The mitral valve's central components are the anterior and posterior leaflet, the annulus and the subvalvular apparatus. The latter two connect the valve to the left ventricular (LV) endocardium. The annulus is a ring-like fibrous entity with a 3D shape resembling a saddle (fig. 1 and 2), with the middle portions of the anterior annulus being elevated out of the annular plane towards the left atrium (LA) and merging into the aortic mitral curtain. The aortic mitral curtain ends in the left and right fibrous trigone. The posterior leaflet is divided through slits into several scallops (fig. 1). Multiple nomenclatures exist, most commonly the scallops are named P1 to P3 with opposing segments A1 to A3.[13] The mitral commissures are the points where both leaflet's free edges join. They do not coincide with the mitral annulus. The subvalvular apparatus consists of the chordae tendinae and the papillary muscles. The function of the mitral valve is to

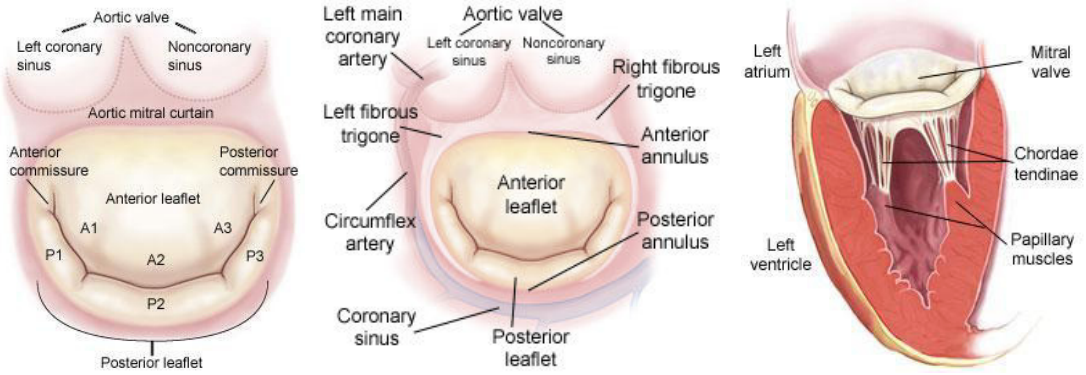

Figure 1: Morphological sketches depicting the view on the mitral valve from the left atrium (left & center image) and cross section of the mitral valve, left atrium & ventricle depicting the papillary muscles and chordae (right image).[14] Reproduced with permission of the authors.

allow blood to flow only one way, from the LA to the LV, separating them hemodynamically. It is opened by the contracting papillary muscles, which are pulling down the leaflets during diastole and remains closed by the ventricular pressure during systole.

The proposed model includes the trigones, commissures, leaflet tips and a posteroannular midpoint modeled as landmark points. Furthermore the leaflets are modeled by Non uniform rational B-spline (NURBS) surfaces,[15] while the annulus is implicitly modeled by the upper leaflet margins which point to the LA. These components together with topological and geometrical constraints define a physiologically compliant model of the mitral valve. The two leaflets, expressed as NURBS paraboloids, are fixed to each other on the line from the respective commissure to the annulus. This way they form a cylinder collapsible at it's bottom, simulating the opened and closed state of the mitral valve. They furthermore are constrained by the landmark points mentioned above.

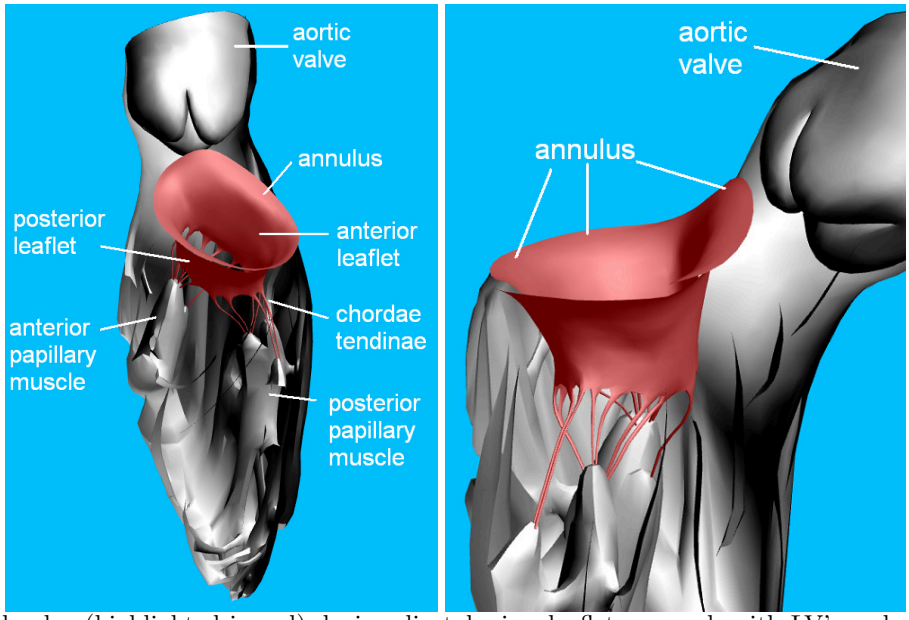

Figure 2: mitral valve (highlighted in red) during diastole, i.e. leaflets opened, with LV's endocardial wall and aortic valve. Note the saddle shape of the annulus visible in the right figure with an elevation towards the aortic valve.

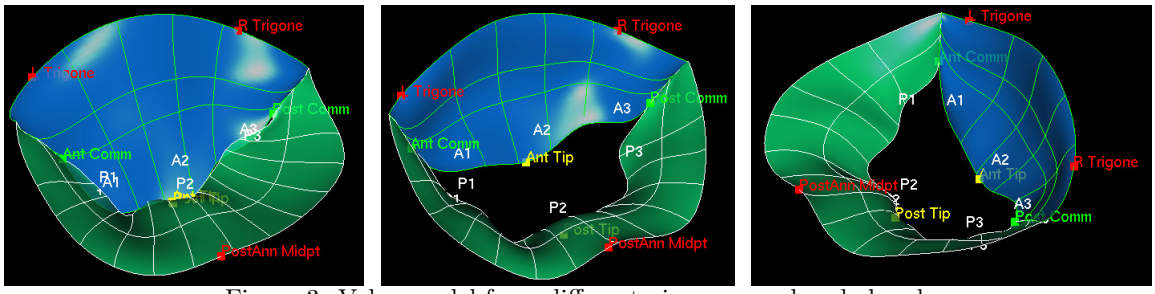

Figure 3: Valve model from different views opened and closed.

$$\underbrace{C^j(u,v)}_{u,v\in[0,1]} = \frac{\sum_{k=0}^{n}\sum_{l=0}^{m} N_{k,d}(u)N_{l,e}(v)w_{k,l}\vec{P^{c,j}_{k,l}}}{\sum_{k=0}^{n}\sum_{l=0}^{m} N_{k,d}(u)N_{l,e}(v)w_{k,l}} \qquad j = \begin{cases} 0: & \text{anterior leaflet} \\ 1: & \text{posterior leaflet} \end{cases} \tag{1}$$

with C as the j^{th} leaflet surface, $\vec{P^{c,j}_{k,l}}$ as control points, $w_{k,l}$ as corresponding weights and $N_{k,d}(u)$ and $N_{l,e}(v)$ as the d^{th} and e^{th} degree B-splines basis functions defined on the non-periodic knot vector U and V, respectively. The surfaces passes through the trigone points $\vec{L}^{tri}_{j}$, commissure points $\vec{L}^{comm}_{l}$, leaflet tips $\vec{L}^{tip}_{l}$ and

the posteroannular midpoint $\vec{L}^{pam}$, which is expressed by the following equations:

$$C^j(u_l^{tip}, 1) = \vec{L}_j^{tip} \quad (2)$$

$$C^j(0, 1) = \vec{L}_j^{comm} \quad (3)$$

$$C^j(1, 1) = \vec{L}_{(l+1) \bmod 2}^{comm} \quad (4)$$

$$C^0(u_i^{tri}, 0) = \vec{L}_j^{tri} \quad (5)$$

$$C^1(u^{pam}, 0) = \vec{L}^{pam} \quad (6)$$

The two leaflets C^0 and C^1 are fixed to each other on the line from the respective commissure to the annulus, i.e. their isolines at parametric values $v = 0$ and $v = 1$ coincide:

$$C^j(1, v) = C^{(j+1) \bmod 2}(0, v) \quad (7)$$

The annulus is the joint isocurve at parametric value $u = 0$ for both leaflet surfaces. Fig. 4 illustrates the above discussed constraints and relations. A comprehensive description of NURBS is given by Piegl *et al.*[15]

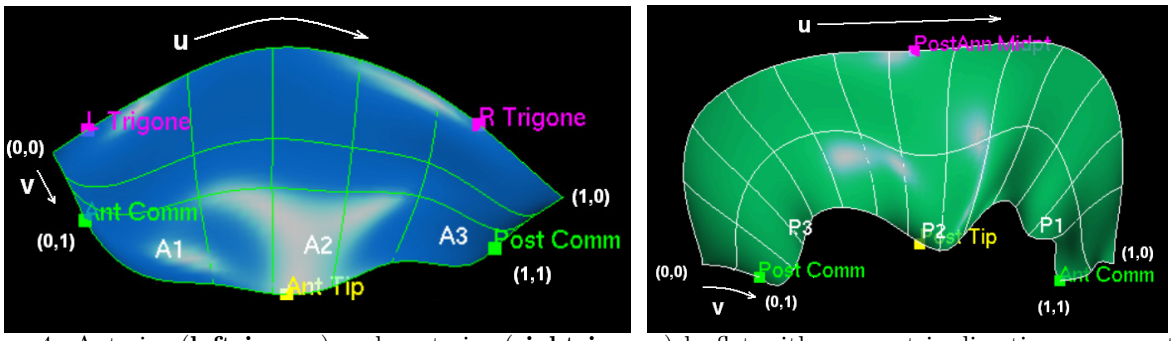

Figure 4: Anterior (**left image**) and posterior (**right image**) leaflet with parametric directions, parameteric values (u,v) at corner points and spatial relations with landmarks.

3. MODEL ESTIMATION

In order to estimate a patient-specific instance of the model the landmark points and NURBS control points have to be determined in a four-dimensional Euclidean space (3D+time), cumulating into $3T(7 + 240)$ parameters*. Estimation of such high dimensional parameter vector is a difficult task, thus we propose to first detect a similarity transformation, followed by landmark locations and then fully fit the model and estimate the dynamics applying recent advances in discriminative learning and incremental searching techniques. Fig 5 gives an overview on the overall segmentation procedure and the applied techniques.

3.1 Rigid Parameters

The similarity transformation $\Theta = (X, Y, Z, \theta, \phi, \psi, S_X, S_Y, S_Z)$ is detected using the marginal space learning approach (MSL),[16] which has proven to be a robust and reliable method. To find the bounding box describing the valve's location (X, Y, Z), orientation – described by the Euler angles (θ, ϕ, ψ) – and size (S_X, S_Y, S_Z) (fig. 6(a)) a probabilistic boosting tree (PBT)[17] is used in conjunction with Haar and steerable features.

As within our framework the object localization task is formulated as a classification problem, discriminative classifiers are used to exhaustively test all possible rigid parameter hypotheses Θ and find the hypotheses with high probability for the given volume. The classifiers based on the PBT, which learns the target distribution by exploiting a divide-and-conquer strategy, are trained from a manually annotated database.

*with T discrete time steps (6 to 15 for a regular 4D ultrasound scan), 7 landmarks and 240 NURBS control points

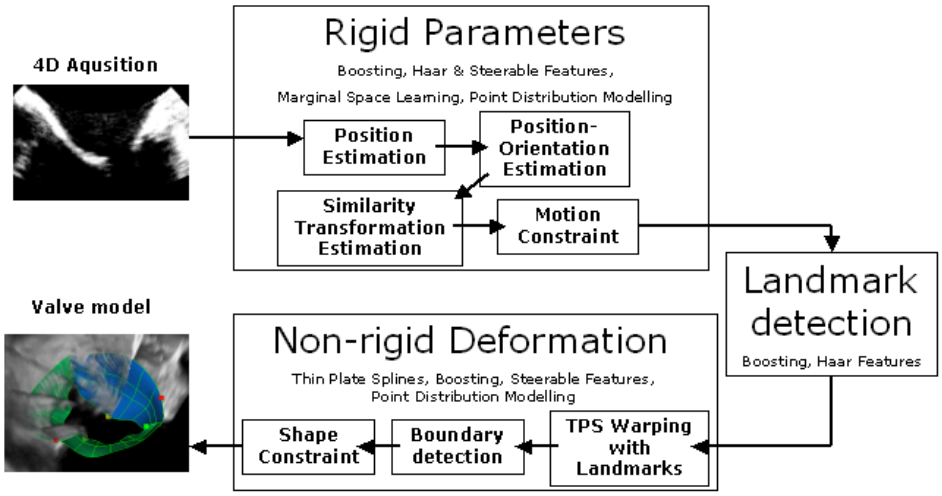

Figure 5: Block diagram of the segmentation pipeline alongside with the utilized machine learning techniques.

Exhaustive searching of course keeps us from getting stuck in local optima. As each hypothesis consists of nine parameters however, we have to tackle the curse of dimensionality to cope with the large set of hypotheses. Therefore we use the MSL approach and instead of using one single classifier directly to scan the complete space of rigid parameters, we exploit the observation of a clustered parameter space. Thus the idea is to incrementally learn and apply classifiers on projected sample distributions. With increasing dimensions, the search space is pruned by previous marginal space classifiers. Therefore the estimation is split into three problems (fig. 5):

- translation estimation,
- translation-orientation estimation
- full similarity transformation estimation

After each step, the best candidates are kept and augmented with multiple hypotheses for the next stage, i.e. after translation estimation the candidates are augmented with orientation hypotheses and after translation-orientation estimation, the candidates are augmented with scale hypotheses.

Besides reducing the searching space, we can also use different features or learning methods in each step. While in the translation estimation step, efficient 3D Haar features are used (since we treat rotation as an intra-class variation), in the translation-orientation and similarity transformation estimation steps steerable features are applied in order to avoid volume rotation, while still exploiting the advantages of global features.

The basic idea of steerable features is to sample some points from the volume under a special pattern and local features are computed at each sampling point, such as voxel intensity and the gradient, its components, its length, its projection onto a given vector and angles between gradient and a given vector. The sampling pattern is steered - i.e. rotated and scaled - , instead of aligning the volume to a given orientation to extract Haar wavelet features, which is why this type of features is called steerable features. As each feature is local, it is easy to compute and therefore efficient, but the sampling pattern is global to capture the orientation and scale information. Thus it combines the advantages of both global and local features.

3.2 Landmark Locations

Similarly to the estimation of the valve's rigid parameters, a PBT-based discriminative classifier H_{L_i} is trained and applied for each landmark point $\vec{L}_i = (x_i, y_i, z_i)$, which utilizes Haar features. As the valve's rigid parameters are known from the previous detection stage, it is not necessary to scan the complete volume I for the location of L_i. Instead each landmarks' search space $\mathcal{D}_i$ is defined by a search range given by a box relative to the detected

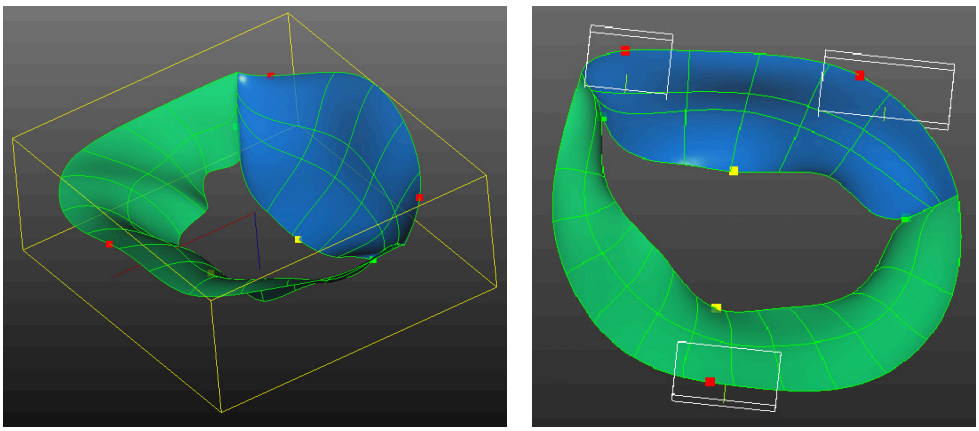

(a) bounding box (b) landmark search ranges

Figure 6: Mitral valve model with (a) bounding box (yellow lines) and (b) landmark search ranges for the mitral trigones. The red and blue line indicate the x- and z-direction respectively within the local coordinate system given by the bounding box, the orientation is thereby derived from the landmark points. The landmark search ranges are relative to the previously detected bounding box.

bounding box (fig. 6(b)). Thus the probability of the presence of landmark i computed at each location inside the domain $\mathcal{D}_i$ within the image I is given by:

$$p(\vec{L}_i|x_s, y_s, z_s, I) = H_{L_i}(x_s, y_s, z_s|I) \quad , \quad (x_s, y_s, z_s) \in \mathcal{D}_i \tag{8}$$

At training stage these search ranges are computed and normalized by the volume resolution and the valve's similarity transformation, obtained from the ground truth. The training set is completely drawn from the search range as this is the only relevant domain for this detection task.

3.3 Non-rigid Deformation

For mapping the mean shape to the volume I the detected landmarks $\vec{L}_i^d$ and their corresponding counterparts $\vec{L}_i^m$ on the mean shape $\bar{\vec{x}}$ have to be matched. As this is due to inter-patient variability usually not feasible with a linear transform, a thin-plate-spline (TPS) transform[18,19] is performed, to optimally capture all kinds of anatomical variations.

The resulting model estimate provides a quite accurate global fitting of the model, however it requires further local processing for precise object delineation. Therefore in the next step, we increase the degrees of freedom of the model in order to capture the true anatomical morphology of the valve. The parameteric surfaces are sampled to obtain a set of discrete boundary locations, each of which needs to be transformed individually.

An intuitive approach would be to move each point along its respective surface normal towards high gradients in the vicinity of the point, as usually abrupt variations in the image's intensity constitute an object's boundary as proposed for active shape models (ASM).[20] However especially for the case of Ultrasound as we have noisy object boundaries and signal dropout, this does not work quite satisfying. Learning based methods perform better as shown in[21–25] when applied not only with gradients at different image resolutions but also with intensities and by incorporating local neighborhood. Therefore we train and use a learning based boundary detector and use steerable features to guide the shape deformation.

The boundary detector is applied to a set of N discrete boundary locations $\vec{Q}_i$ each along their respective surface normal $\vec{n}_i$. These are obtained by uniformly sampling the parameter space of the K parametric surfaces $C^j(u, v)$ of the TPS transformed mean model. The boundary detector H_B is then used to test a set of hypotheses, which are drawn along the normals $\vec{n}_i$ at each of the discrete boundary locations $\vec{Q}_i$. The new boundary point

$\vec{Q}'_i$ is set to the hypothesis with maximal probability as determined by the classifier H_B:

$$s' = \arg\max_{s \in S} H_B(\vec{Q}_i + s\,\vec{n}_i|I) \quad (9)$$

$$\vec{Q}'_i = \vec{Q}_i + s'\,\vec{n}_i \quad (10)$$

where s and s' are scalars determining the displacement of $\vec{Q}_i$ along the normal $\vec{n}_i$ and the search range S was heuristically determined through the segmentation error after model transformation.

After boundary detection, segmentation results is constrained using a point distribution model (PDM).[20] As the rigid parameters are already known and the surfaces are fixed to the detected landmark points, only one single projection is necessary in contrast to the iterative approach of Active Shape Models.[20] In our case the goal is to remove boundary point outliers and spatial noise only.

The final estimation is obtained by fitting the parametric model to the refined samples by solving a linear least squares problem.[26]

3.4 Dynamics

To estimate the valve's dynamics we follow a physiology-driven strategy assuming that the motion stays within certain ranges which can be estimated from the training set. Therefore the above procedure is repeated for each following time frame with the difference that the bounding boxes' and landmark detectors are scanned over a neighborhood – precomputed at training stage – starting from the initial result, leading to a significant performance boost and minimizing error propagation at the same time. Fig. 7 shows a typical motion sequence for the case of the mitral valve.

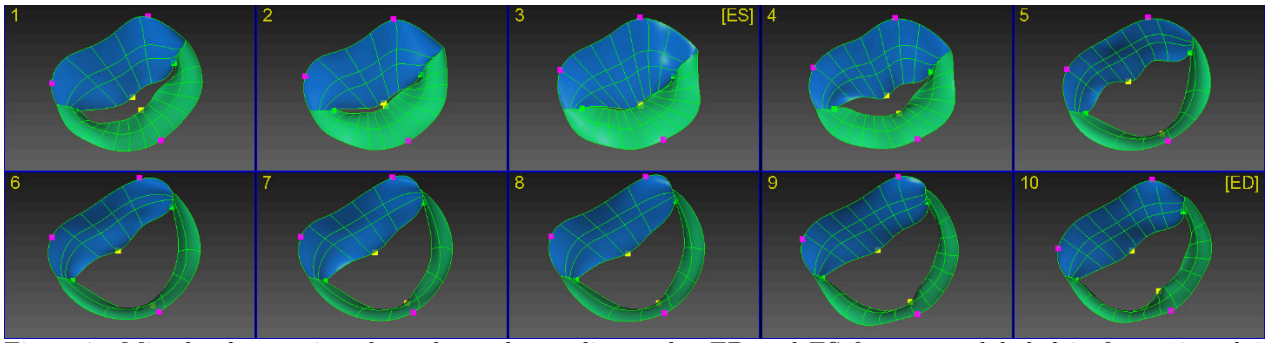

Figure 7: Mitral valve motion throughout the cardiac cycle. ED and ES frames are labeled in fram 10 and 3 respectively.

To increase the robustness of the estimation of rigid parameters and landmark locations, motion models are applied after each step. Both are basically a PDMs extended to motion and constructed specifically for the bounding boxes' corner points and landmark points respectively. Therefore not only point coordinates from a single time step but a fixed number of time steps T are concatenated into the high dimensional vectors $\vec{x}_i$ for estimation of and processing by motion model:

$$\vec{x}_i = (x_{1,1}, \ldots x_{N,T}, y_{1,1}, \ldots y_{N,T}, z_{1,1}, \ldots z_{N,T})^T \in \mathbb{R}^{3N \cdot T} \quad (11)$$

with $N = 8$ for the bounding box corner points. It is important to note that the cyclic motion patterns are registered onto the cardiac phases, which are the end-diastolic (ED) and end-systolic (ES) phases of the hearts cycle. These have been manually labeled during manual segmentation of a particular 4D acquisition.

Furthermore as the bounding box already encodes the similarity transform we simply use this information for registering motion patterns onto each other instead of applying GPA on estimation of the motion model. Analogously steps are taken on projection.

4. RESULTS

4.1 Results on valve model estimation

The estimation performance evaluation is done on 3D+time trans-esophageal echocardiogram data acquired from 30 patients affect by various valvular diseases. A total of 350 volumes were obtained using heterogeneous capture ranges and each frame of the sequences were associated to a manually generated annotation considered to be the ground truth. Rotational acquisitions have been converted to cartesian volumes with isotropic resolution ranging between 0.6 to 1 mm. The volumes contain $136 \times 128 \times 112$ to $160 \times 160 \times 120$ voxels. The scans are acquired from different patients affected by various cardiovascular diseases.

The results of the 3-fold cross-validation for full model fitting are shown in table 1. The model estimation precision was evaluated with respect to the ground truth using the point-to-mesh measurement. This is computed by averaging the distance between each sample point from the detected model and the closest sample point from the ground-truth model. In order to guarantee symmetry, the measurement is also computed vice-versa, from the ground-truth to the detected model. These two quantifications are averaged and provide the error measurement.

Fig. 8 show the results of each step of our mitral valve segmentation pipeline in an Ultrasound volume in different views. It can easily be observed from both fig. 8 and table 1 how the precision of the segmentation gradually increases with each step.

The overall mean accuracy is 2.82 mm at an average overall detection speed of 43 seconds (2.20 GHz CPU, 2.0 GB RAM).

	Mean	Median	90%
Rigid	4.29	4.33	6.23
Landmark	2.93	2.91	4.14
Boundary	2.82	2.39	3.31

Table 1: Mean, median and 90-percentile value of the test error in millimeters for fully fitted mitral model using the point-to-mesh error measurement after each segmentation step – i.e. similarity transformed mean shape after rigid parameter estimation, TPS transformed mean shape after landmark detection and fully fitted model after boundary refinement.

4.2 Results on clinical valve evaluation

The quantitative capabilities of the model are demonstrated by comparing a set of morphological and dynamic model-based measurements to literature reported valve dimensions. Any given measurement can easily be derived and automatically computed from the proposed geometric model in a straightforward manner, as the relevant anatomic parts and landmarks are explicitly modeled. Quantitative evaluation is performed on Ultrasound images of regurgitant mitral valves with mild stenosis. Table 2 summarizes the evaluation results and demonstrates the precision of the proposed model-based quantization method.

	AA (cm^2)	APD (cm)	AL-PM-D (cm)	AC (cm)	TV (mL)	MVA (cm^2)
Mean	10.5	3.2	3.6	11.7	6.2	3.2
Std dev	1.7	0.35	0.34	0.9	1.5	0.8
Mean in literature	11.2[8,9]	2.8[27,28]	3.1[27]	12.8[8]	4.09[8]	1.5-5.0[1]
Std dev in literature	0.6	0.2	0.1	1.4	1.2	

Table 2: Mean and standard deviation of respective measurements provided by the model in comparison to mean values for accordingly diseased subjects in literature.

Mitral annular dimensions - annular area (AA), anteroposterior (APD) and anterolateral-posteromedial diameters (AL-PM-D) and annular circumference (AC) - as well as tenting volume (TV) are of interest for patients with regurgitant mitral valves, while the mitral valvular orifice area (MVA) is also used to assess the severity stenotic valves.[1,2,29] Table 2 provides mean and standard deviation of the mentioned measurements derived from our model as well as values from literature for accordingly diseased subjects. For MVA the mild stenosis is evident as the value has to lie between 1.5 (severe stenosis) and 5.0 cm^2 (healthy subject).

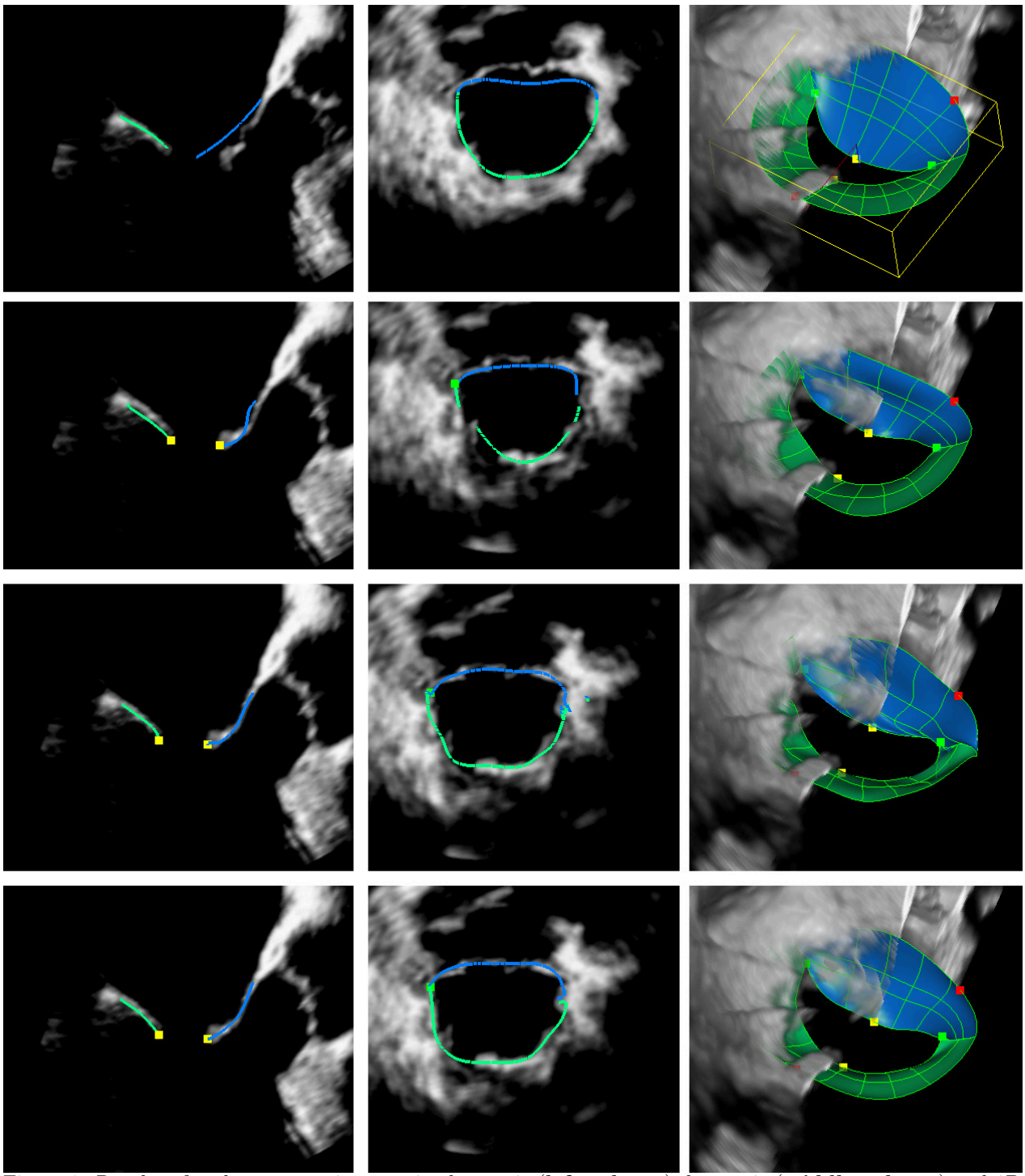

Figure 8: Results of each segmentation step in short-axis (**left column**), long-axis (**middle column**) and 3D view (**right column**). The box detection provides a rough estimate of the valve location, orientation and size (**first row** with rigidly transformed mean model). It is refined by the detected landmark locations and the mean model is warped onto the detected landmark points with TPS (**second row**). This quite accurate fitting is refined by boundary detection (**third row**), however the result is quite noisy and needs to be smoothed by constraining the shape with a PDM (**fourth row**). We recommend to view this figure in color in the electronic version of the proceedings.

5. CONCLUSION

In this paper we proposed a novel method for quantitative and visual evaluation mitral valve, based on a dynamic model estimated from 4D ultrasound sequences. A robust and computationally efficient algorithm, which combines learning-based technologies into a coarse-to-fine approach, was proposed for estimating a patient specific valve model from imaging data. Automatic model-based measurements provide a significant advance in morphological and functional clinical evaluation of the mitral valve. Our method overcomes the limitations of mentioned related work, which concentrates on very specific phenomena and fails to deliver such integrated and flexible approach.

REFERENCES

[1] Bonow, R. O., Carabello, B. A., Chatterjee, K., de Leon, A. C. J., Faxon, D. P., Freed, M. D., Gaasch, W. H., Lytle, B. W., Nishimura, R. A., OGara, P. T., ORourke, R. A., Otto, C. M., Shah, P. M., and Shanewise, J. S., "ACC/AHA 2006 Guidelines for the Management of Patients With Valvular Heart Disease," *Circulation* **114**, e84 – e231 (2006). http://dx.doi.org/10.1161/CIRCULATIONAHA.106.176857.

[2] Vahanian, A., Baumgartner, H., Bax, J., Butchart, E., Dion, R., Filippatos, G., Flachskampf, F., Hall, R., Iung, B., Kasprzak, J., Nataf, P., Tornos, P., Torracca, L., and Wenink, A., "Guidelines on the management of valvular heart disease: The task force on the management of valvular heart disease of the european society of cardiology," *Eur Heart J* **28**(2), 230–268 (2007). http://dx.doi.org/10.1093/eurheartj/ehl428.

[3] Bartlett, J. W. and Frost, C., "Reliability, repeatability and reproducibility: analysis of measurement errors in continuous variables," *Ultrasound in Obstetrics and Gynecology* **31**(4), 466–475 (2008). http://dx.doi.org/10.1002/uog.5256.

[4] Nkomo, V., Gardin, J., Skelton, T., Gottdiener, J., Scott, C., and Enriquez-Sarano, M., "Burden of valvular heart diseases: a population-based study," *Lancet* (2006). http://dx.doi.org/10.1016/S0140-6736(06)69208-8.

[5] Votta, E., Maisano, F., Bolling, S., Alfieri, O., Montevecchi, F., and Redaelli, A., "The geoform disease-specific annuloplasty system: A finite element study," *Ann Thorac Surg* **84**, 92–101 (2007). http://dx.doi.org/10.1016/j.athoracsur.2007.03.040.

[6] Peskin, C. S. and McQueen, D. M., "Fluid dynamics of the heart and its valves," in [*Case Studies in Mathematical Modeling: Ecology, Physiology, and Cell Biology*], Othmer, H., Adler, F., Lewis, M., and Dallon, J., eds., 309–337, Prentice-Hall, Englewood Clifs, NJ, USA (1996).

[7] Kuai, X., Zhang, J., Ren, B., Liu, F., Gong, G., and Zeng, Y., "Stress analysis on stentless quadrileaflet pericardial mitral valve," *Communications in Numerical Methods in Engineering* (2007). http://dx.doi.org/10.1002/cnm.999.

[8] Watanabe, N., Ogasawara, Y., Yamaura, Y., Kawamoto, T., Toyota, E., Akasaka, T., and Yoshida, K., "Quantitation of mitral valve tenting in ischemic mitral regurgitation by transthoracic real-time three-dimensional echocardiography," *J Am Coll Cardiol* **45**, 763–769 (2005). http://dx.doi.org/10.1016/j.jacc.2004.11.048.

[9] Ahmad, R., Gillinov, A., McCarthy, P., Blackstone, E., Apperson-Hansen, C., Qin, J. X., Agler, D., Shiota, T., and Cosgrove, D. M., "Annular geometry and motion in human ischemic mitral regurgitation: Novel assessment with three-dimensional echocardiography and computer reconstruction," *Ann Thorac Surg* **78**, 2063–2068 (2004). http://dx.doi.org/10.1016/j.athoracsur.2004.06.016.

[10] Song, J., Fukuda, S., Kihara, T., Shin, M., Garcia, M., Thomas, J., and Shiota, T., "Value of mitral valve tenting volume determined by real-time three-dimensional echocardiography in patients with functional mitral regurgitation.," *American Journal of Cardiology* **98**(8), 1088–1093 (2006). http://dx.doi.org/10.1016/j.amjcard.2006.05.036.

[11] Timek, T., Dagum, P., Lai, D., Liang, D., Daughters, G., Tibayan, F., Ingels, N., and Miller, D., "Tachycardia-induced cardiomyopathy in the ovine heart: Mitral annular dynamic three-dimensional geometry," *Journal of Thoracic and Cardiovascular Surgery* **125**(2), 315 – 324 (2003). http://dx.doi.org/10.1067/mtc.2003.80.

[12] Hammer, P., Vasilyev, N., D.P., P., del Nido, P., and Howe, R., "Fast image-based model of mitral valve closure for surgical planning," in [*MICCAI 2008 Workshop Proceedings: Computational Biomechanics for Medicine III*], 15–26 (2008). http://www.mech.uwa.edu.au/CBM2008/.

[13] Anderson, R. H. and Kanani, M., "Mitral valve repair: critical analysis of the anatomy discussed," *Multimedia Manual of Cardiothoractic Surgery* (2006). http://dx.doi.org/10.1510/mmcts.2006.002147.

[14] Carpentier, A., Adams, D., and Filsoufi, F., [*Carpentier's Techniques of Valve Reconstruction*], W.B. Saunders, Philadelphia (in press). Figures are from http://www.mitralvalverepair.org, which are modified from the book.

[15] Piegl, L. and Tiller, W., [*The NURBS book*], Springer-Verlag, London, UK (1995).

[16] Zheng, Y., Barbu, A., Georgescu, B., Scheuering, M., and Comaniciu, D., "Fast automatic heart chamber segmentation from 3d ct data using marginal space learning and steerable features," in [*ICCV*], (2007). http://dx.doi.org/10.1109/ICCV.2007.4408925.

[17] Tu, Z., "Probabilistic boosting-tree: Learning discriminative models for classification, recognition, and clustering," in [*ICCV '05: Proceedings of the Tenth IEEE International Conference on Computer Vision*], 1589–1596, IEEE Computer Society, Washington, DC, USA (2005).

[18] Duchon, J., "Interpolation des fonctions de deux variables suivant le principe de la flexion des plaques minces," *RAIRO Analyse Numerique* **10**, 5–12 (1976).

[19] Bookstein, F. L., "Principal warps: Thin-plate splines and the decomposition of deformations," *IEEE Trans. Pattern Anal. Mach. Intell.* **11**(6), 567–585 (1989).

[20] Cootes, T. F., Taylor, C. J., Cooper, D. H., and Graham, J., "Active shape models - their training and application," *Computer Vision and Image Understanding* **61**(1), 38–59 (1995).

[21] Zheng, Y., Barbu, A., Georgescu, B., Scheuering, M., and Comaniciu, D., "Four-chamber heart modeling and automatic segmentation for 3d cardiac ct volumes using marginal space learning and steerable features," *IEEE Trans. on Medical Imaging* **27**(11), 1668–1681 (2008). http://dx.doi.org/10.1109/TMI.2008.2004421.

[22] Yang, L., Zheng, Y., Georgescu, B., Meer, P., and Comaniciu, D., "3d ultrasound tracking of the left ventricles using one-step forward prediction and data fusion of collaborative trackers," in [*Proc. IEEE Conf. Computer Vision and Pattern Recognition*], (2008).

[23] Dollar, P., Tu, Z., and Belongie, S., "Supervised learning of edges and object boundaries," in [*Proc. CVPR*], 19641971 (2006).

[24] van Ginneken, B., Frangi, A., Staal, J., ter Haar Romeny, B., and Viergever, M., "Active shape model segmentation with optimal features,," *IEEE Trans. Medical Imaging,* **21**(8), 924933 (2002).

[25] Martin, D., Fowlkes, C., and Malik, J., "Learning to detect natural image boundaries using local brightness, color and texture cues," *IEEE Trans. Pattern Anal. Machine Intell.* **26**(5), 530549 (2004).

[26] DeBoor, H., [*A practical guide to splines*], Springer, New York (1978). ISBN: 0-387-90356-9.

[27] Kwan, J., Shiota, T., Agler, D., Popovic, Z., Qin, J. X., Gillinov, M. A., Stewart, W. J., Cosgrove, D. M., McCarthy, P. M., and Thomas, J. D., "Geometric differences of the mitral apparatus between ischemic and dilated cardiomyopathy with significant mitral regurgitation," *Circulation* (2003). http://dx.doi.org/10.1161/01.CIR.0000053558.55471.2D.

[28] Yu, H.-Y., Su, M.-Y., Liao, T.-Y., Peng, H.-H., Lin, F.-Y., and Tseng, W.-Y. I., "Functional mitral regurgitation in chronic ischemic coronary artery disease: Analysis of geometric alterations of mitral apparatus with magnetic resonance imaging," *J Thorac Cardiovasc Surg* **128**, 543–551 (2004). http://dx.doi.org/10.1016/S0002-8703(00)90077-2.

[29] Filsoufi, F., Rahmanian, P., Anyanwu, A., and Adams, D., "Physiologic basis for the surgical treatment of ischemic mitral regurgitation," *Am Heart Hosp J* **4**(4), 261–268 (2006). http://dx.doi.org/10.1111/j.1541-9215.2006.05932.x.